Hydrobiologia (2024) 851:1723–1739
https://doi.org/10.1007/s10750-023-05411-3

PRIMARY RESEARCH PAPER

Holocene limnological changes in saline and freshwater lakes, Lower Nhecolândia, Pantanal, Brazil

Giliane Gessica Rasbold · Luiz Carlos Ruiz Pessenda · Paulo Eduardo De Oliveira · Elton Eduardo Novais Alves · Dayana Rodrigues Silva · Hudson W. Carvalho · José Albertino Bendassolli · Célia Regina Montes · Adolpho Jose Melfi · Michael M. McGlue

Received: 28 May 2023 / Revised: 13 October 2023 / Accepted: 14 October 2023 / Published online: 20 November 2023

Abstract The lower Nhecolândia region, in the south of the Pantanal, contains thousands of shallow freshwater and saline-alkaline lakes isolated by sandy ridges. To understand the paleoenvironment, sediment cores from B02SR (freshwater) and 07SR (saline-alkaline) lakes were analyzed, employing a combination of ^{14}C dating, microfossils, geochemical, elemental, and isotopic analyses. The 07SR core recovered Late Pleistocene sediments (~23,440 cal yrs BP), and the B02SR core Middle Holocene sediments (~6080 cal yrs BP). The base of the cores consists of bedded sands with no organic matter, sponge spicules, or diatoms. Phytoliths suggest the presence of *cerrado* vegetation with seasonal floods, suggestive of a periodically inundated distal floodplain. We interpret that the two lakes sustain perennial alkaline geochemical conditions between ~3080 and ~1330 cal yrs BP. The Lake B02SR transitioned to slightly acidic waters with low electrical conductivity from ~1330 cal yrs BP to the present, probably associated with a connection to ephemeral shallow or perennial channels. Lake 07SR maintained consistent water chemistry throughout the record, suggesting that an isolated drainage pattern remained unchanged creating persistent alkaline conditions. Our results suggest that lake chemical changes were spatially variable in lower Nhecolândia in the Holocene, which has implications for ecosystem services.

Keywords Wetlands · Shallow lakes · Diatoms · Phytoliths · Tropical paleoecology

Handling editor: Jasmine Saros

G. G. Rasbold (✉) · M. M. McGlue
Department of Earth and Environmental Sciences, University of Kentucky, Lexington, KY, USA
e-mail: grasbold@uky.edu

L. C. R. Pessenda · D. R. Silva · H. W. Carvalho · J. A. Bendassolli
Center for Nuclear Energy in Agriculture, University of São Paulo, Piracicaba, São Paulo, Brazil

P. E. De Oliveira
Institute of Geosciences, University of São Paulo, São Paulo, São Paulo, Brazil

P. E. De Oliveira
The Field Museum of Natural History, Chicago, IL, USA

E. E. N. Alves
Chair in Soil Science, Mohammed VI Polytechnic University, Benguerir, Morocco

C. R. Montes · A. J. Melfi
Institute of Energy and Environment, University of São Paulo, São Paulo, São Paulo, Brazil

Introduction

The Pantanal is considered the largest tropical wetland on the planet, covering an area of approximately 135,000 km^2 in the central region of South America (Por, 1995; Merino & Assine, 2020; Keddy et al., 2009). It is famous for its seasonal flood pulse, which

transforms large areas of the basin and provides critical habitat and refuge for wildlife and a diverse flora (Junk & Cunha, 2005; Tortato & Izzo, 2017; Girard et al., 2010). The Pantanal is composed of complex lentic and lotic ecosystems, including lakes of different origins, swamps, networks of both active and ancient fluvial channels, and large distributary fans (Lo et al., 2019; Assine & Soares, 2004; McGlue et al., 2016). Many morphological features of the Pantanal are relics of a complex history of environmental changes that occurred since the end of the Pleistocene (Assine, 2003; Novello et al., 2019). Among these diverse landscapes, the region of lower Nhecolândia stands out for its thousands of shallow freshwater and saline lakes, ephemeral channels, and sandy, tree-covered ridges. Most of these lakes are small and semi-rounded or elongated; locally called *baías* (freshwater) or *salinas* (saline-alkaline waters). The origins of these lakes, their hydrochemistry and spatial arrangement have intrigued scientists for many years (Barbiero et al., 2002; Furquim et al., 2010; Furian et al., 2013; Bergier et al., 2016).

Some of what is known about the environmental history of the Pantanal comes from paleolimnological studies of floodplain lakes. Sediment cores from lakes on the Paraguay River floodplain have been studied using biological and geochemical indicators of hydroclimate change, including analyses of sponge spicules, pollen, diatoms, elemental and light stable isotopes, and biomarkers (Whitney et al., 2011; McGlue et al., 2012; Metcalfe et al., 2014; Fornace et al., 2016; Bezerra et al., 2019; Rasbold et al., 2019, 2021). However, unlike the floodplain lakes connected to the Paraguay River, many of the saline-alkaline Nhecolândia lakes are isolated from each other by sandy ridges called *cordilheiras* (Fig. 1). These features are elevated up to 5 m above the *vazantes*, and flood waters rarely reach the ridge crests, which tend to be densely vegetated (Costa et al., 2015).Because they are isolated, they offer the potential for intact

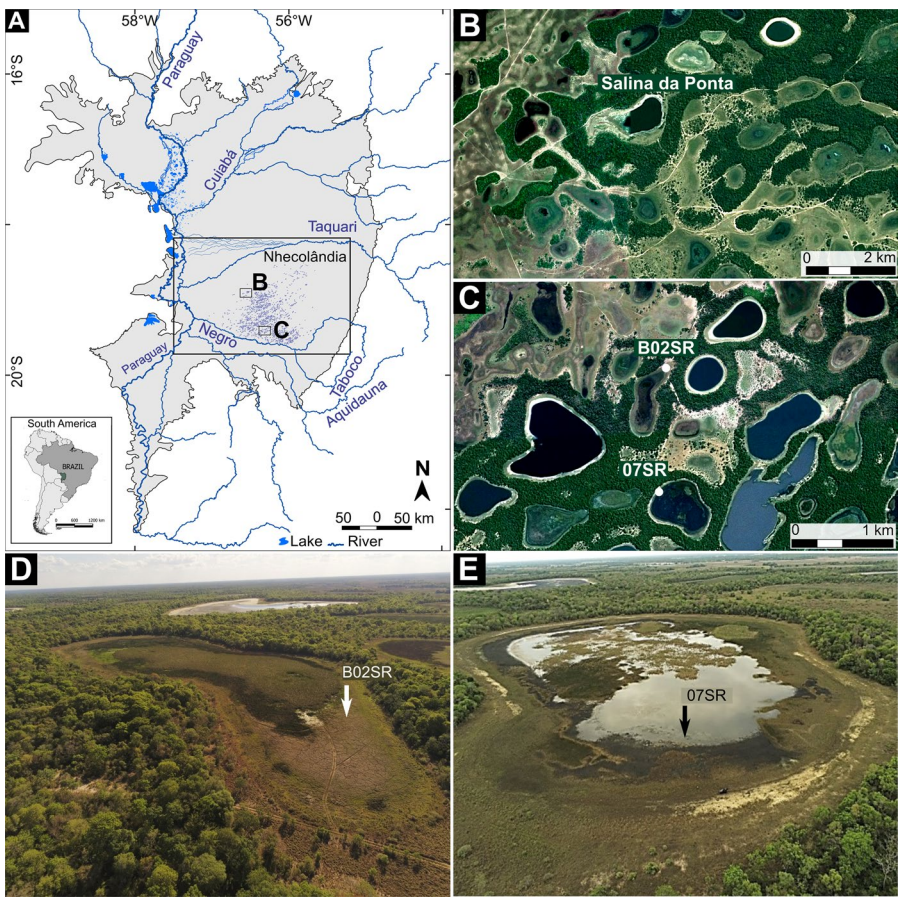

Fig. 1 **A** Map of the Pantanal wetlands highlighting the location of the Nhecolândia in the southern portion of the Taquari River megafan; **B–C** Satellite image detail shows the landscape and the locations of the Salina da Ponta Lake (Guerreiro et al., 2018), B2SR Lake, 07SR Lake; **D**. Freshwater lake, the white arrow indicates the B02SR core sampling location; **E** Saline-alkaline lake, the black arrow indicates the 07SR core sampling location; Source: João Godinho/2020 (drone overflight)

sedimentary records. Paleolimnological research on these types of lakes is still very limited but has shown that depositional setting and lake water chemistry changes have occurred in the late Pleistocene and Holocene (McGlue et al., 2017; Becker et al., 2018; Guerreiro et al., 2018) (Fig. 1B). In contrast, studies on the freshwater lakes of Nhecolândia are not available; integration of these lakes into the seasonal drainage network has most likely constrained the use of their sediments for environmental reconstructions. In this study, we test the hypothesis that hydrochemical changes can be detected in lake sediments from lower Nhecolândia (Fig. 1B). We employed extensive multiproxy analyses on the sediments of both a saline-alkaline and a freshwater lake, to understand the evolution of these environments and the interactions among climate, vegetation, and hydrology. The lower Nhecolândia lake district provides valuable ecosystem services, some of which are tied to lake water chemistry (e.g., carbon sequestration, certified organic ranching opportunities, etc.). Therefore, the results of the study hold importance for conservation planning, in addition to a more robust understanding of the response of shallow aquatic ecosystems to global climatic change.

Geologic and environmental setting

The Nhecolândia sub-region of the Pantanal is an abandoned depositional lobe of the Taquari River megafan, covering an area of 29,000 km^2 (Zani et al., 2012). The Taquari River flows from east to west, draining the Brazilian plateau and reaching the Pantanal lowlands before its confluence with the Paraguay River. Nhecolândia is delimited by the Rio Negro in the south and the Paraguay River in the west (Fig. 1). Lower Nhecolândia is characterized as a geomorphological compartment of fluvio-lacustrine plains made up of Cenozoic-aged alluvial sediments (Lacerda Filho et al., 2006). The climate of this region is tropical semi-humid, with two well-defined seasons, a dry season during the austral winter (May to September, mean rainfall of ~ 180 mm) and a rainy season during the austral summer (October to April, mean rainfall of ~ 855 mm) (Furian et al., 2013). Lower Nhecolandia is a complex fluvial-lacustrine environment with ~ 15,000 saline-alkaline and freshwater shallow lakes of 1–2 m deep with unstratified water columns (Mourão et al., 1988; Barbiero et al., 2002; Rezende-Filho et al., 2012). There are also river channels known as *vazantes* and *corixos*, which act as distributive channels during the seasonal flood pulse. *Vazantes* are ephemeral, shallow channels that are activated for the outflow of flood waters, while *corixos* are perennial shallow channels.

The vegetation community in the Nhecolândia region can be divided into five main ecological groups according to their distribution and environmental characteristics (Becker et al., 2018): (i) The *vazantes* contain grasses, trees, and shrubs over the seasonally flooded areas, which includes species of Poaceae, Cyperaceae, Asteraceae, Arecaceae, Melastomataceae, Anacardiaceae, *Polygala* sp.; *Gomphrena* sp.; *Anadenanthera* sp.; *Tabebuia* sp., Anacardiaceae, *Tapirira guianensis* Aubl., and *Copernicia alba* Morong; (ii) The *cordilheiras* are covered by trees and shrubs typical of the central Brazilian savanna (*cerrado*), with species of Poaceae, Cyperaceae, Anacardiaceae, *Anadenanthera* sp.; *Tabebuia* sp., and *Attalea phalerata* Mart. ex Spreng.; (iii) The shorelines of saline-alkaline lakes contain *Copernicia alba*, *Tabebuia* sp., *Gomphrena* sp., Bromeliaceae, and Asteraceae; (iv) Freshwater lakeshores are colonized by herbs and shrubs adapted to moist soils, such as Cyperaceae, Poaceae, *Typha domingensis* Pers., and *Cabomba piauhiensis* Gardner; (v) Several communities characterized by monodominance can be found surrounding the sandy ridges of the lakes, such as the *Carandazal*, which has the dominant species *Copernicia alba* (Arecaceae), the *coronal* dominated by *Elyonorus muticus* (Spreng.) Kuntze (Cyperaceae), and *gravatal* dominating by Bromeliaceae of the species *Bromelia balansae* Mez.

Materials and methods

Sediment core X-ray, color, and (geo)chronology

A 200-cm-long sediment core (B02SR) was recovered from a dry freshwater lake basin at 19º23′07.8″S; 56º20′01.01″W, and a 150-cm-long sediment core (07SR) was recovered at 19º23′54.6″S; 56º19′50.1″W, in a saline-alkaline lake, using a Russian sediment borer. The cores were sealed in the field and transported to the ^{14}C Laboratory at the Center for Nuclear Energy in Agriculture, University of São Paulo (CENA-USP). The cores were photographed and

x-radiographed to identify the stratigraphy and sedimentary structures. Sediment colors were determined by visual comparison with Munsell® Chart standards (Company, 1975). Fifteen sediment organic matter samples were dated by accelerator mass spectrometry (AMS) radiocarbon dating at the Center for Applied Isotope Studies at the University of Georgia, USA (Table 1). Samples were physically and chemically pre-treated according to the methodology described by Pessenda et al. (2009). Bayesian age-depth models for cores B02SR and 07SR were constructed using the Bacon for R package (Blaauw & Christen, 2011), the SHCal20 calibration curve (Hogg et al., 2020) and the post-bomb SH Zone 1–2 curve (Hua et al., 2022). Radiocarbon dates are reported as the median probability age (cal yr BP). We analyzed sediment grain size following the Wentworth (1922) distribution. Subsamples were dried, weighed, and oxidized with hydrogen peroxide (35%) at 80 ℃ to remove organic matter and a 4% HCl solution to eliminate carbonates. They were then sieved with a 1 mm mesh cloth, dried and remaining grains weighed. We dispersed the rest of the material using ultrasound before determining grain size via laser diffraction with a Shimadzu Sald 2201 Laser Particle Size analyzer.

X-ray Fluorescence (XRF) analysis

The B02SR sediment core was placed in 75 mm in diameter PVC cradles and the surface was covered with a 2.5 µm-thick Mylar® film (Chemplex, Palm City, USA). Geochemical analysis was performed using a portable energy-dispersive X-ray fluorescence spectrometer (pED-XRF—model Tracer III-SD, Bruker AXS, Madison, USA). The pED-XRF was fixed on a support and positioned on top of the core and its film covering. The pED-XRF and support were moved every 1 cm along the length of the core. The XRF spectra were obtained by the program S1PXRF v. 3.8.3. The analyses were performed under atmospheric pressure, with the X-ray tube operating at 40 kV and 20 µA, with a dwell time of 30 s per analysis, and a dead time of less than 12%. The net intensities and background of each x-ray line were obtained from the Bayesian deconvolution using ARTAX v. 7.4. The net intensity of Rh Kα Compton radiation was determined in the energy range (ROI) of 19.2–19.8 keV. Intensities of characteristics X-ray of each chemical element were normalized by Rh Kα Compton. The XRF normalized data versus core depth data were plotted to evaluate the accumulation

Table 1 Radiocarbon dates used in the age-depth model from B2SR and 07SR

ID	Depth (cm)	Lab code*	Age (pMC)	Error (±)	2-σ range (cal yr AD)	Median Probability (cal yr AD)	Material
B2SR	5–7	51848[a]	102.015	0.717	1957–1956	1957	Bulk
ID	Depth (cm)	Lab code*	Age (^{14}C yr BP)	Error (±)	2-σ range (cal yr BP)	Median Probability (cal yr BP)	Material
B2SR	25–23	51,849	1839	34	1825–1610	~1720	Bulk
B2SR	34–32	54,230	2718	61	2960–2710	~2800	Bulk
B2SR	45–43	51,850	2995	85	3350–2880	~3120	Bulk
B2SR	107–105	54,225	2620	25	2760–2520	~2730	Bulk
B2SR	161–159	54,226	5120	130	6185–5585	~5830	Bulk
B2SR	177–176	56,244	5130	50	5990–5660	~5820	Bulk
B2SR	195–194	56,245	4630	40	5465–5050	~5310	Bulk
07SR	16–14	51,862	353	26	450–300	~390	Bulk
07SR	34–32	51,863	2485	52	2710–2355	~2530	Bulk
07SR	66–64	54,231	4140	70	4830–4420	~4630	Bulk
07SR	82–80	51,865	4863	28	5600–5470	~5530	Bulk
07SR	96–95	54,232	5490	45	6390–6020	~6240	Bulk
07SR	132–130	54,233	8324	52	9450–9030	~9290	Bulk
07SR	146–144	51,867	19,460	56	23,750–23150	~23,410	Bulk

*Accelerator mass spectrometry (AMS) of center for applied isotope studies of university of Georgia

of the chemical elements during sedimentation. The X-ray data were exported into the program PAST v 3.22 (Hammer et al., 2001) to perform the principal component analysis (PCA). First, the data were normalized to obtain the arithmetic mean equal to zero and standard deviation equal to one, using the equation $[(x-\bar{x})/\sigma]$, where x is the chemical element content at a given depth, $\bar{x}$ is the average content of the entire profile, and σ is the standard deviation of the entire profile.

Isotopic and elemental analysis

Sediment sub-samples were collected every 4 cm along the length of both cores for total organic carbon (TOC), total nitrogen (TN), $\delta^{13}C$, and $\delta^{15}N$ measurements. Each sediment sample was freeze-dried and pre-treated according to (Buso Junior et al., 2013). To determine the modern stable carbon isotope signature of the most representative modern plant species were collect near the sampling points. We analyzed 15 plants, washed the leaves with deionized water, dried them at 40° C, and ground them. The isotope values from plants and sediments were measured at the Stable Isotope Laboratory of CENA/USP using an IRMS Delta V Advantage isotope ratio mass spectrometer interfaced with combustion set. The $\delta^{13}C$ values (‰) were expressed with respect to the VPDB standard and $\delta^{15}N$ (‰) in relation to the atmospheric N_2 standard, with a standard deviation of ± 0.2 ‰. The results of TOC and TN are expressed as percentages of dry weight and *C/N* values calculated accordingly (Lorente et al., 2014). These data were used to identify the sources of organic matter, which can be produced by lacustrine algae, aquatic macrophytes, and C3 and C4 land plants (Meyers, 1994).

Phytoliths, sponge spicules, diatoms

Sediment sub-samples (1 cm^3) were analyzed for siliceous microfossils, following complete organic matter digestion with 35% H_2O_2 on a hot plate at 60 ℃ (Battarbee et al., 2001). To estimate phytolith concentration, two tablets of an exotic marker (37.168 cm^{-3}) were added to the samples, including 10 ml of hydrochloric acid (10%) to assist with dissolution. Microscope slides were mounted with Naphrax, a medium permanent high-refractive index (1.7). Slides were analyzed at 1000× magnification with a light microscope. When possible, at least 200 diatom valves were identified from each sample interval. Diatom frustules were identified and counted at the genus level, following the taxonomy of Metzeltin & Lange-Bertalot (2007), de Souza Santos et al. (2012), Malone et al. (2012), Morales et al. (2014), Tremarin et al. (2014), and Guerreiro et al. (2018). Taxonomic identification of sponge spicules was performed through systematic observations of at least 200 spicules, distinguishing among the different sponge skeletal elements, including megascleres, gemmuloscleres, and microscleres. Identification of different species followed the key of Class Demospongiae Sollas (1885), Order Spongillida Manconi and Pronzato 2002 to Neotropical Freshwater Sponge Species (Pinheiro & Calheira, 2020) and the morphological guide of neotropical freshwater sponge spicules for paleolimnological studies (Rasbold et al., 2023). Plant phytoliths were counted to at least 200 fossils per sample, with morphological identifications following the International Code for Phytolith Nomenclature 2.0 (ICPT, 2019).

Pollen grains and charcoal

Subsamples (1 cm^3) for the B02SR were processed, following the protocol described in Collinvaux et al. (1999): addition of one spike of exotic *Lycopodium clavatum* L. spores (Batch number: 177,745, Lund University, 2008) to determinate pollen and spore concentrations (Collinvaux et al., 1999). The procedure was based on the addition of HF to remove silicate minerals, KOH and acetolysis to remove humic acids and the organic contents within palynomorphs. At least 300 terrestrial pollen grains were counted per sample using a ZEISS photomicroscope at 1000x. Identification was based on the literature (Salgado-Labouriau, 1973; Absy, 1975; Faegri et al., 1989; Roubik & Moreno, 1991; Collinvaux et al., 1999) and the modern pollen reference collection of the ^{14}C Laboratory (CENA/USP). Pollen diagrams were plotted using TiliaGraph® and CONISS to stratigraphically constrained cluster analysis (Grimm, 1987).

For macroscopic charcoal analysis, subsamples of 1 cm^3 were collected at intervals of 2 cm for 07SR core ($n = 75$), and processed following the sieving method (Millspaugh & Whitlock, 1995). Each subsample was submerged in deflocculant (5% solution of sodium hexametaphosphate) for 24 h and then

carefully washed through a 150 µm sieve to remove fine organic and inorganic materials. The counts of the charcoal fragments retained in the sieves were carried out using a stereomicroscope × 10–15. The resulting dataset was converted to charcoal concentration (number of charcoal particles per cm^{-3}).

Results

Age model and modern vegetation

The core from the freshwater lake (B02SR) is composed at its base of Middle Holocene-aged sediments (~6080 cal yrs BP), and the upper 110 cm of the core corresponds to the Late Holocene. Sedimentation rates in the core range from ~0.5 mm/yr in the basal portion (200–50 cm) and ~0.02 cm/yr in the upper portion of the core (50–0 cm) (Table 1 and Fig. 2). The core from the saline-alkaline lake (07SR) dates at its base to the Late Pleistocene (~23,440 cal yrs BP) (Table 1 and Fig. 2). Moving up the section, the radiocarbon dates represent Early Holocene ages (~9290 cal yrs BP, 132 cm), the sedimentation rates ~0.093 mm/yr in the basal portion between 145 and 132 cm, suggesting a hiatus in the interval.

Carbon isotope analysis of plants colonizing lakes shorelines and *cordilheiras* indicate a community composed of C3 plants ($\delta^{13}C$ between − 32 ‰ and − 22 ‰), made up of trees and some grasses (Poaceae) (Fig. 3). One sample (Bromeliaceae), which is a Crussalaceae Acid Metabolism (CAM) plant, had a $\delta^{13}C$ value of − 14.2‰. The B02SR lake is predominantly vegetated by the species *Typha domingensis*, which has a $\delta^{13}C$ value of − 29.5 ‰.

B02SR core (Freshwater Lake)

The lithology, granulometry, TOC, TN, $\delta^{13}C$, $\delta^{15}N$, and elemental geochemistry of the B02SR core are shown in Figs. 3 and 4, whereas the microfossils are in Fig. 5. The results of the pED-XRF analysis and the evaluation of the first (PC1–55.7% of the explained variance) and second (PC2–25.1% of the explained variance) principal components scores of the PCA suggest three units for the B02SR core.

Unit I (200–50 cm; ~6080–3080 cal yr BP)

Unit I is composed predominantly of very dark brown, massively bedded, medium and fine-grained sands. The variance of the pED-XRF data is explained by the positive scores of PC2 (25.1%),

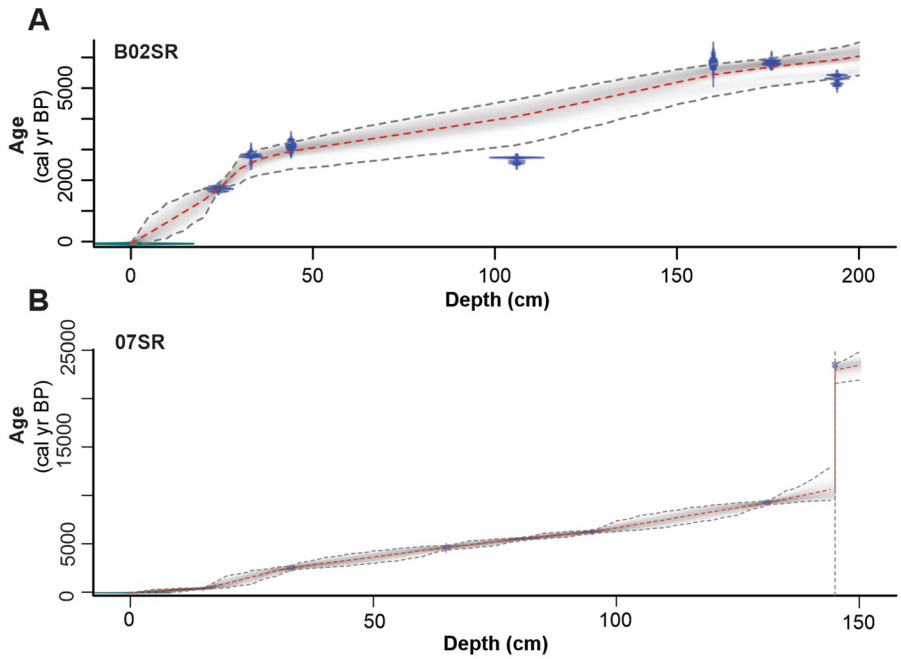

Fig. 2 Age-depth models based on Bayesian statistics for **A** core B02SR core and **B** core 07SR. Blue markers denote ^{14}C dated layers. One dated layer was excluded by Bacon at B02SR core. Dashed lines indicated the 95% confidence interval

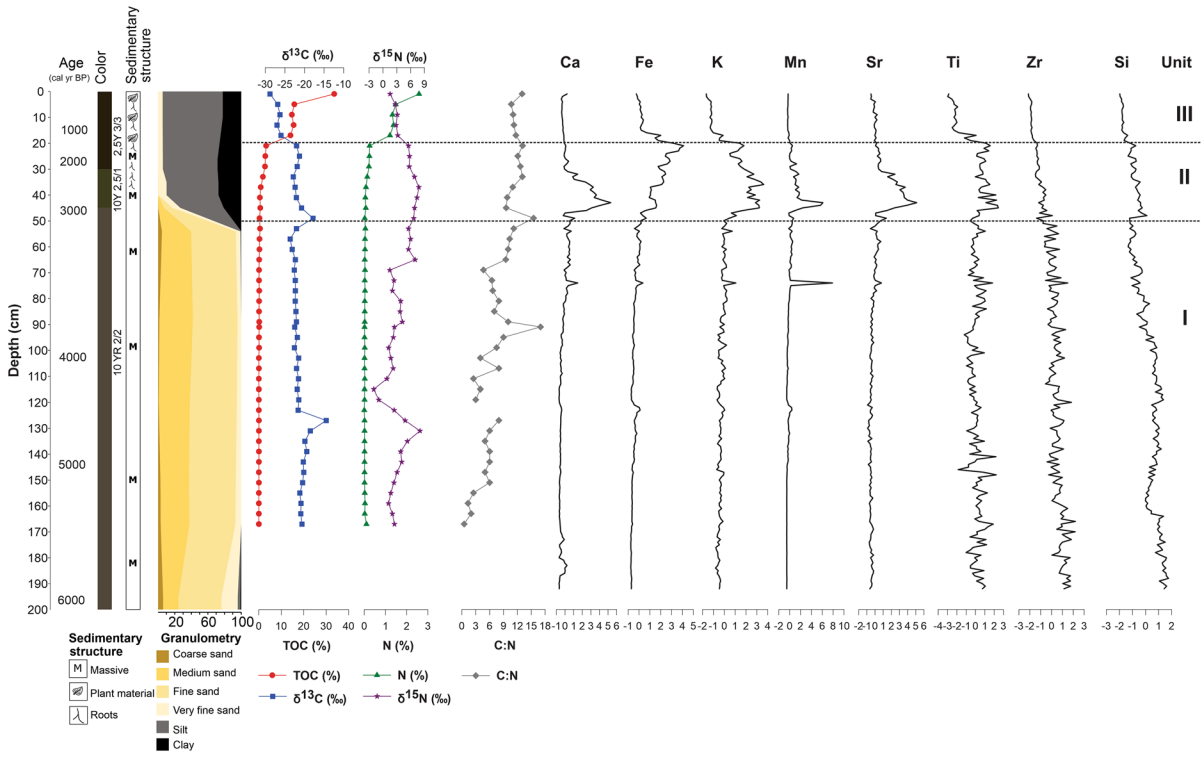

Fig. 3 B02SR core stratigraphy, granulometry, total organic carbon (TOC), $\delta^{13}C$, total nitrogen (TN), $\delta^{15}N$, and C: N values (weight/weight), Intensities of characteristics X-ray of each chemical element normalized by Rh Kα Compton versus depth data

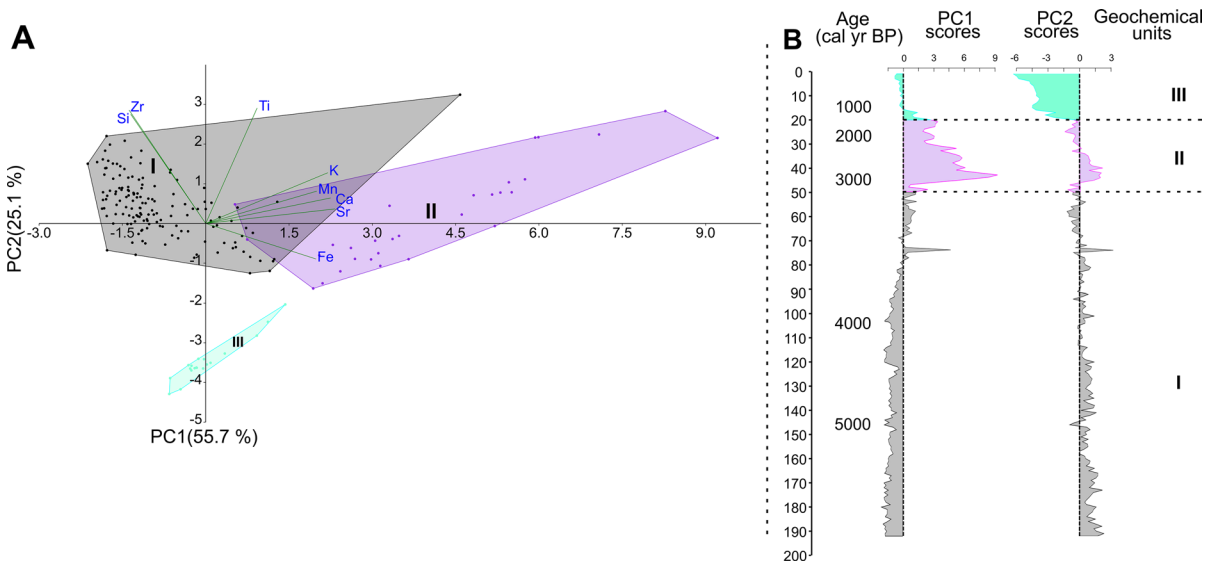

Fig. 4 **A** Principal components biplot for the chemical elements determined by pED-XRF; **B** Plot of PC1 (55.7% of the explained variance) versus PC2 (25.1% of the explained variance) scores vs B02SR core depth (cm)

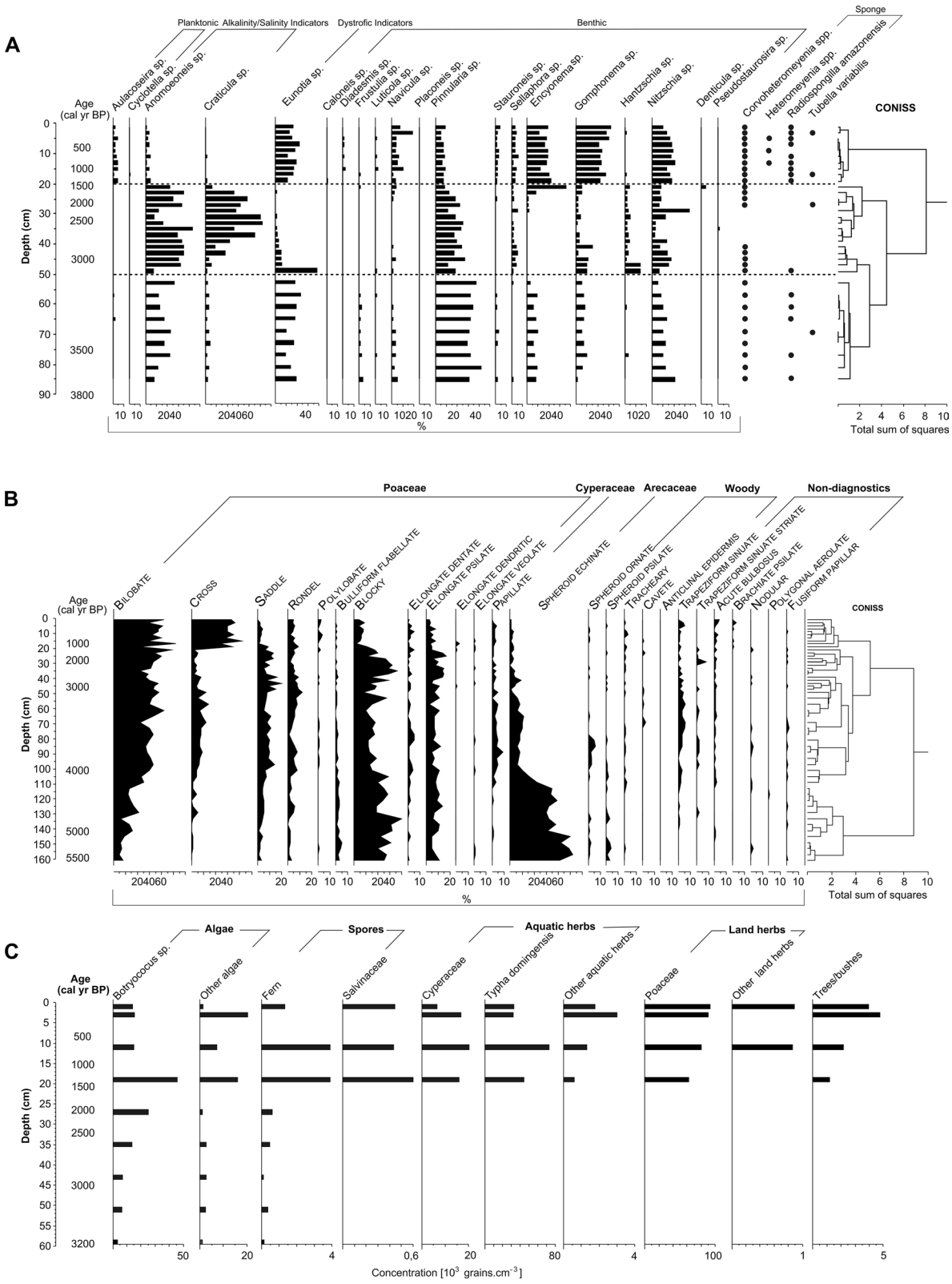
A
Planktonic
Alkalinity/Salinity Indicators
Dystrofic Indicators
Benthic
Sponge
Aulacoseira sp.
Cyclotella sp.
Anomoeoneis sp.
Craticula sp.
Eunotia sp.
Caloneis sp.
Diadesmis sp.
Frustulia sp.
Luticola sp.
Navicula sp.
Placoneis sp.
Pinnularia sp.
Stauroneis sp.
Sellaphora sp.
Encyonema sp.
Gomphonema sp.
Hantzschia sp.
Nitzschia sp.
Denticula sp.
Pseudostaurosira sp.
Corvoheteromeyenia spp.
Heteromeyenia spp.
Radiospongilla amazonensis
Tubella variabilis
Age (cal yr BP)
Depth (cm)
CONISS
%
Total sum of squares
B
Poaceae
Cyperaceae
Arecaceae
Woody
Non-diagnostics
Bilobate
Cross
Saddle
Rondel
Polylobate
Bulliform flabellate
Blocky
Elongate dentate
Elongate psilate
Elongate dendritic
Elongate veolate
Papillate
Spheroid echinate
Spheroid ornate
Spheroid psilate
Tracheary
Cavete
Anticlinal epidermis
Trapeziform sinuate
Trapeziform sinuate striate
Acute bulbosus
Brachiate psilate
Nodular
Polygonal aerolate
Fusiform papillar
Age (cal yr BP)
Depth (cm)
CONISS
%
Total sum of squares
C
Algae
Spores
Aquatic herbs
Land herbs
Botryococcus sp.
Other algae
Fern
Salviniaceae
Cyperaceae
Typha domingensis
Other aquatic herbs
Poaceae
Other land herbs
Trees/bushes
Age (cal yr BP)
Depth (cm)
Concentration [10^3 grains.cm^-3]

◂**Fig. 5** Quantification and identification of biological indicators for the B02SR core. **A** Relative abundance of diatom and sponge spicules; **B** Relative abundance of phytoliths; **C.** Concentrations of algae, spores, and pollen grains. See text for details

represented by high characteristic radiation intensities of Si and Zr (Fig. 3). Silicon is probably associated with quartz-rich sandy layers and Zr with weathering-resistant zircons connected by high energy-related depositional processes. Mn concretions were identified and detected by XRF through high intensity of Mn Kα line (peaks seen in Mn profile—Fig. 3). The C and N contents are close to 0%. There were not enough diatom frustules or sponge spicules for quantification between 200 and 90 cm. Between 90 and 50 cm, the diatom community was composed predominantly of *Pinnularia* sp., *Eunotia* sp., *Nitzschia* sp. and *Anomoeoneis*sp. It was possible to identify the presence of the sponge species *Corvoheteromeyenia* sp., *Radiospongilla amazonensis* Volkmer-Ribeiro & Maciel, 1983, and *Tubella variabilis* (Bonetto & Ezcurra de Drago, 1973). The assemblage of spicules was chiefly composed of fragmented microscleres, with < 5 complete gemmoscleres per horizon. Between 160 and 90 cm, there was 40–60% of phytoliths characteristic of the family Arecaceae and Bromeliaceae (Spheroid echinate). Between 90 and 50 cm, the phytolithic assemblage was composed of grass silica short-cell phytoliths (GSSCP) morphologies produced by grasses (Bilobate, Cross, Saddle and Rondel). Morphologies produced by Poaceae were also identified, but without a specific taxonomic pattern (Blocky, Bulliform Flabellate and elongate entire). It was not possible to identify the pollen assemblies, as grain concentrations were insufficient.

Unit II (50–20 cm; ~ 3080–1330 cal yr BP)

Unit II comprises a transition facies from sandy sediments into silt-rich sediments with a greenish black color. The variance of the pED-XRF data is explained by the negative scores of PC1 axis (~ 56%) and is related to the high relative characteristic radiation intensities of K, Mn, Ca, Sr, and Fe (Fig. 4). In Unit II, the values of TOC were < 3%, the mean $\delta^{13}C$ value is − 22 ‰ (C3 plants predominance), and N remain close to 0% (Fig. 3)., comprising between 35 and 70% of the assemblage. Between 40 and 30 cm, *Craticula* sp. was ~ 50% of the community (Fig. 5). *Anomoeoneis* sp. is tolerant to a wide salinity gradient and is considered euryhaline; however, *Craticula* sp. is usually observed in brackish waters with high electrical conductivity and high pH (i.e., saline-alkaline waters). It was possible to identify only *Corvoheteromeyenia* spp. sponge spicules, with the occurrence of one gemmulosclere. The predominant phytolith morphologies in Unit II were those produced by grasses of the Poaceae family (BILOBATE) and without a specific taxonomic pattern (BLOCKY, BULLIFORM FLABELLATE, and ELONGATE ENTIRE). It was not possible to identify the pollen assembly as the concentrations of grains were insufficient. However, it was possible to identify the presence of green algae, especially *Botryococcus* sp. (Fig. 5).

Unit III (20–0 cm; ~ 1330 cal yr BP–present)

Unit III is composed of silty mud with roots and coarse plant material with dark olive brown color. The variance of the pED-XRF data in this layer is explained by the negative scores of PC2 axis (~ 25%), whose characteristic radiation intensities of Ti, Zr, and Si are diagnostic but are lower than Units I and II (Fig. 4). These lower values may be indicative of a decrease in energy-related depositional processes. The concentration of TOC increases towards the top of the unit, with values up to ~ 35% near the surface; the mean $\delta^{13}C$ was -30 ‰, indicative of C3 plants. The mean TN values are ~ 2.5%, with $\delta^{15}N > 5$ ‰ and C: N ratio of ~ 10, indicative of aquatic organic matter source (Fig. 3). Unit III is characterized by abundant benthic diatoms: *Gomphonema* sp., *Eunotia* sp., *Encyonem*a sp. and *Nitzschia* sp., commonly found in slightly acidic waters with relatively low to moderate conductivity, consistent with extant conditions (Fig. 5). Sponge spicules of the species *Corvoheteromeyenia spp*., *Radiospongilla amazonensis*, *Tubella variabilis* and *Heteromeyenia* sp. Potts, 1881 were found in Unit III. For the phytoliths, there was a presence of the Bilobate and Cross morphotypes (> 50%), which are associated with plants of the Panicoideae subfamily, that is, grasses adapted to conditions of higher soil moisture (Twiss et al., 1969; Fredlund & Tieszen, 1994; Bremond et al., 2005). The pollen assemblage in this unit was dominated by aquatic and terrestrial

herbs, with abundant *Typha domingenis* and Poaceae, respectively. However, pollen grains from trees and shrubs were identified in the samples at the top of the core. The highest concentrations of *Botryococcus* sp. were recorded at ~ 1300 cal yrs BP.

07SR core (Saline-Alkaline Lake)

The lithology, granulometry, TOC, TN, $\delta^{13}C$, $\delta^{15}N$, microfossils, and elemental geochemistry for the sediments of the 07SR core are shown in Figs. 6 and 7. According to the results obtained by the pED-XRF analysis and the evaluation of the first (PC1–71.4% of

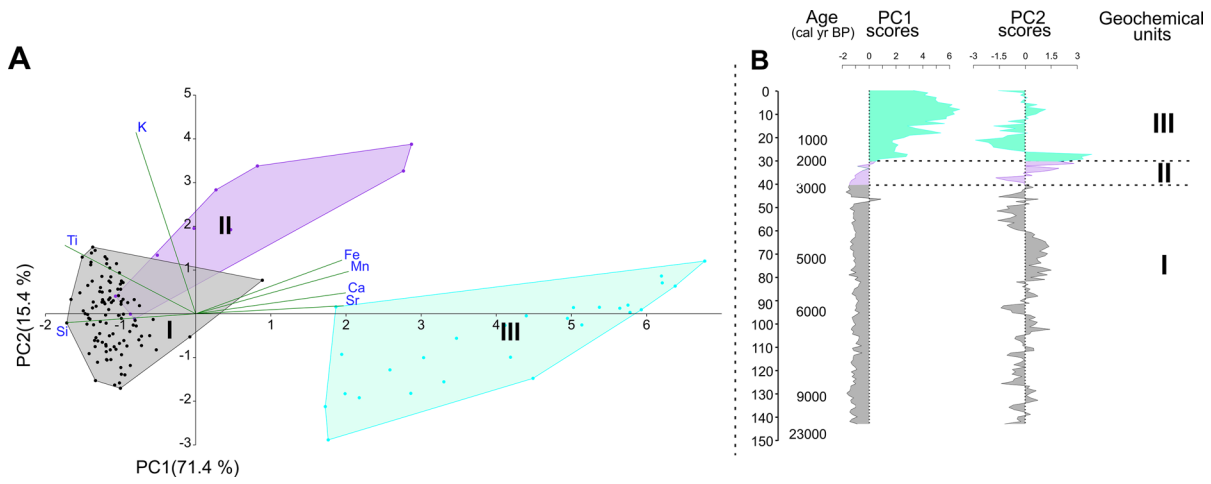

Fig. 6 **A.** Principal components results (PCA biplot) for the chemical elements determined by pED-XRF; **B.** Plot of PC1 (71.4% exp. var.) and PC2 (15.4% exp. var.) scores vs 07SR core depth

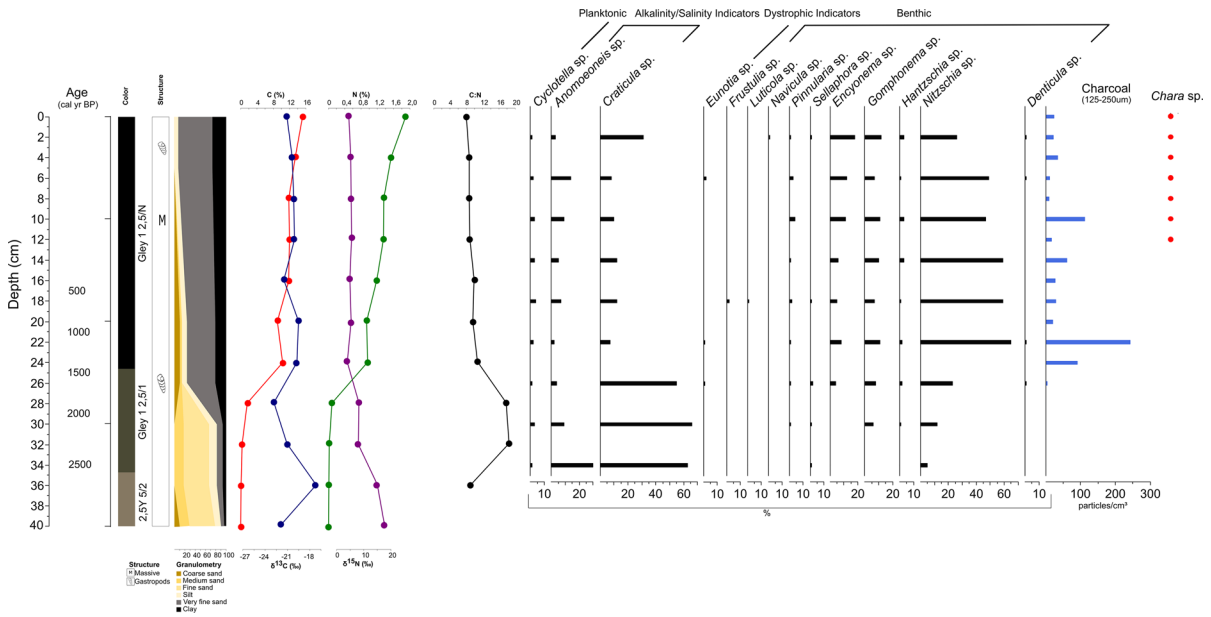

Fig. 7 Stratigraphy, granulometry, total organic carbon (C), $\delta^{13}C$, total nitrogen (N), $\delta^{15}N$, and C: N values (weight/weight), diagram of relative abundance of diatom, and charcoal and *Chara* sp. Presence from 07SR core. Details are described in the text

the explained variance) and second (PC2–15.4% of the explained variance) principal components scores of the PCA, it was possible to distinguish three units for the 07SR core.

Unit I (150–40 cm; ~ 23,440–2990 cal yrs BP)

Unit I correspond to sediments deposited during the interval Early Pleistocene to Late Holocene with low sedimentation and/or sedimentary gap between 145 and 132 cm. It is medium and fine-grained massive sandy bed with Mn-rich concretions. The variance of the pED-XRF data is explained by the negative scores of PC1 axis (~ 71.4%), represented by high characteristic radiation intensities of Si and Ti (Fig. 6). Silicon is probably associated with the quartz in sandy layers and Ti with highly weathering-resistant Ti minerals (e.g., rutile and anatase) in the sediments. The TOC and TN concentrations were negligible in Unit I. It was possible to identify phytoliths characteristic of the Arecaceae and Bromeliaceae families (Spheroid echinate), and woody dicots (Spheroid ornate, Spheroid psilate, and Spheroid facetate). Pollen grains, charcoal particles, diatom frustules, and sponge spicules were not present in Unit I.

Unit II (40–30 cm; ~ 2990–2190 cal yrs BP)

Unit II sediments are chiefly composed of fine sand, with minor accessory silt and clay. The pED-XRF data's variance can be explained by the positive scores of the first and second principal components (PC1 ~ 71.4%; PC2 ~ 15.4%). This loading is linked to a decrease in characteristic radiation intensities of Si and Ti, and an increase in relative intensities of K (Fig. 6). These changes may indicate the beginning of deposition of clay minerals like illite. In this unit, values of TOC were < 1%, the mean $\delta^{13}C$ value is -18 ‰, TN remain close to 0% (Fig. 7). Unit II may be associated with the beginning of the deposition of sediments constituting a saline-alkaline lake. The predominant diatom frustules were *Craticula* sp. (~ 60%), which indicated that during this phase, the lake presented geochemical conditions of brackish waters with high electrical conductivity and hyper/high alkaline pH. It was not possible to identify phytoliths, sponge spicules, pollen grains, and macro charcoal particles in Unit II.

Unit III (30–0 cm; ~ 2190 to present)

Unit III sediments are predominantly composed of silt and clay. The variance of the pED-XRF data in this layer is explained by the positive scores of PC1 axis (~ 71.4%), with high characteristics X-ray intensities of Fe, Mn, Ca, and Sr (Fig. 6). In Unit III, TOC reached ~ 16% and TN is ~ 2% near the core top. The $\delta^{13}C$ values varied between ~ -21 and ~ -19 ‰, which indicates a mixture of C3 and C4 plants. The $\delta^{15}N$ values were ~ 5 ‰, indicating a mixture of terrestrial organic matter and lacustrine phytoplankton (Fig. 7). It was not possible to identify sponge spicules, phytoliths, and pollen grains, however, there is a dominance of *Nitzschia* sp. and *Craticula* sp. diatoms, taxa typical of alkaline environments with moderate to high electrical conductivity. Oogonia of *Chara* sp. (Characeae), were also identified in Unit III, suggesting alkaline water conditions from the last ~ 250 cal yrs BP. It was possible to recover charcoal particles, with the identification of two deposition peaks, the first between ~ 1500 and ~ 1000 cal yrs BP, and the second at ~ 210 cal yrs BP.

Paleoenvironmental interpretations

Core 07SR presents basal sediments from Late the Pleistocene (~ 23,410 cal yrs BP, 144 cm) followed by Early Holocene ages (~ 9290 cal yrs BP, 132 cm), where the low sediment accumulation rate (~ 0.00085 cm/year) was probably associated with a less humid climatic period and/or high precipitation events that removed part of the substrate from the profile. Between the Late Pleistocene and Early Holocene in Pantanal there is evidence of periods with higher rainfall interspersed with lower periods of a weakened monsoon (Whitney et al., 2011; Novello et al., 2016; Bezerra et al., 2019; Rasbold et al., 2019). These changes in precipitation directly influence hydrological dynamics, and consequently the deposition and preservation of sediments. The activation of secondary channels of the Paraguay River in large floodplains lakes resulted in gaps in Late Pleistocene and Early Holocene sediments, indicating a more humid climate, with increased intensity of monsoons and seasonal pulses during this period (Novello et al., 2016; Rasbold et al., 2019). Cores analyzed in Nhecolândia also showed discontinuity in the deposition of sediments, where the actions

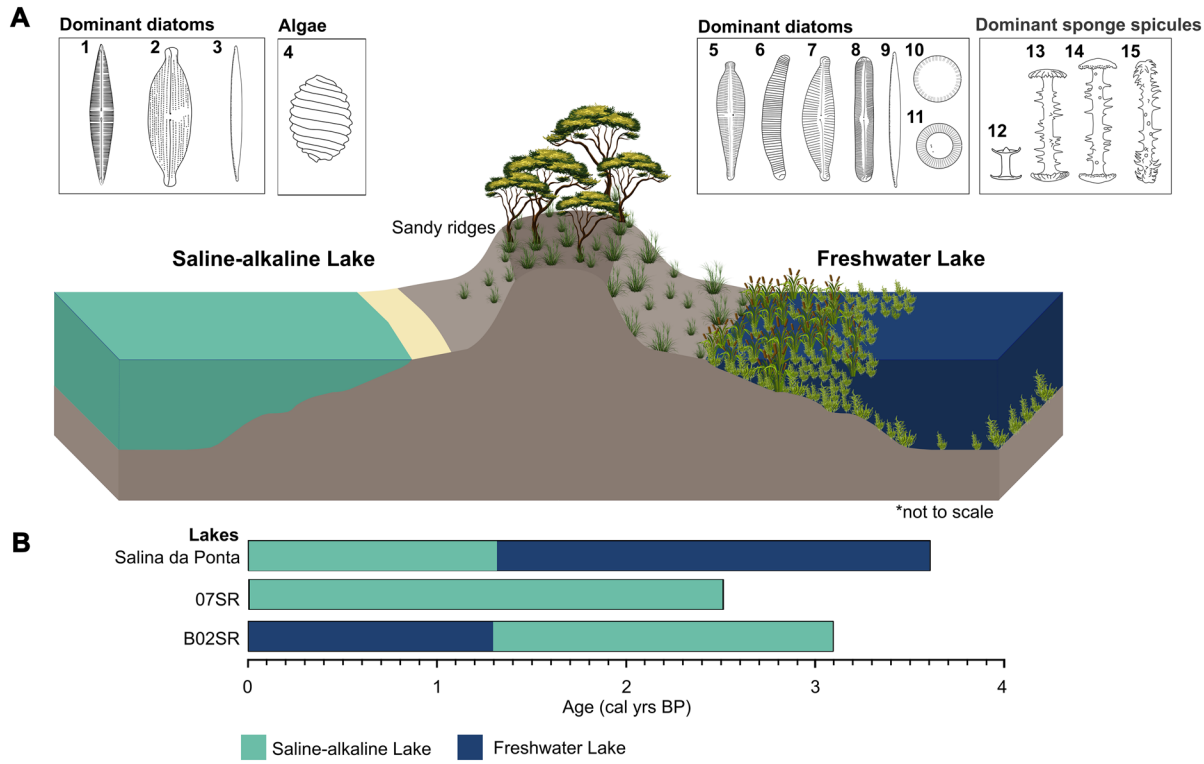

Fig. 8 **A** Conceptual model of sedimentary indicators for saline-alkaline and freshwater lakes in the Nhecolândia Region during the Late Holocene. **Saline-alkaline lake**. Dominant diatoms. **1** *Craticula* sp.; **2** *Anomoeoneis* sp.; **3** *Nitzschia* sp.; **4** Presence oogonia of *Chara* sp. (Characeae). Low or absent sponge spicules. High pED-XRF data for K, Mn, Ca, Sr, and Fe. **Freshwater lake.** Dominant diatoms. **5** *Gomphonema* sp.; **6** *Eunotia* sp.; **7** *Encyonema* sp.; **8** *Pinnularia* sp.; **9** *Nitzschia* sp.; **10** *Aulacoseira* sp.; **11** *Cyclotella* sp.; Dominant sponge spicules. **12** *Tubella variabilis*; **13** *Corvoheteromeyenia* spp.; **14** *Heteromeyenia* sp.; **15** *Radiospongilla amazonensis*. Low pED-XRF data for K, Mn, Ca, Sr, and Fe. **B** Timeline of the lake typologies changes in Salina da Ponta lake (Guerreiro et al., 2018), 07SR Lake, and B02SR Lake

of surface flows could have caused erosion (Assine, 2003). The presence of a sharp lithostratigraphic shift from fine sand and silt to organic-rich mud change, and the incomplete sedimentary records, are evidence of seasonal hydrology, during the Late Pleistocene to Middle Holocene in the lakes across the Nhecolândia (McGlue et al., 2016).

The absence of organic matter (values of TOC and TN ~ 0%) and of sponge and diatom spicules (aquatic indicators), and the preservation of phytoliths of Arecaceae and Bromeliaceae family (Spheroid echinate) and of woody dicotyledons (Spheroid ornate, Spheroid psilate, and Spheroid facetate), indicate that during the Middle to Late Holocene, where today are the freshwater and saline lakes (B2SR and 07SR), possibly was a region with *cerrado* vegetation, with seasonal floods, similar to distal floodplain settings without permanent lakes. Sediment core analyses from floodplain lakes in the Pantanal have indicated a less humid climate than present during the Early and Middle Holocene, with reduced precipitation intensity, leading to a decrease in the flood pulses and levels of these lakes (Whitney et al., 2011; McGlue et al., 2012; Rasbold et al., 2019). This climate change created favorable conditions for the occurrence of fires in non-flooded *cerrado* systems, which are dominated by herbaceous and shrubby vegetation (Power et al., 2016).

The pollen, phytoliths, sponge spicules, diatoms, and macrocharcoal data record the vegetation and aquatic communities (freshwater sponges and diatoms) colonizing the environment, supporting the interpretations regarding the paleovegetation, paleoclimate and paleoecology of the area, especially in the last ~ 3000 cal yrs BP. Lacustrine environments are interpreted to start forming at ~ 3080 cal yrs BP

(B02SR core) and ~ 2500 cal yrs BP (07SR core), with the inception of fine sediments (silt and clay) deposition, possibly under alkaline geochemical conditions as indicated by the diatom communities (Fig. 8). Our XRF data indicates that in the saline-alkaline phases, the sediments contain high relative K, Mn, Ca, Sr, and Fe (Fig. 8). A regional study by Barbiero et al. (2002) conducted on surface and subsurface waters of Nhecolândia revealed that freshwaters in the region are CO_3^{2-}, Cl^-, Na^+, and K^+-rich, whereas saline waters exhibit higher concentrations of CO_3^{2-} and Na^+. As the waters become more saline, pH and alkalinity increase, K^+ decreases slightly, and Mg^{2+} and Ca^{2+} concentrations decrease significantly. Barbiero et al. (2002) concluded that the variability is primarily due to evaporative concentration, and that the precipitation of K^+, Mg^{2+}, and Ca^{2+} in the saline waters occurs through the formation of authigenic carbonates and Mg^{2+}-silicates around the lakes. Biological and geochemical indicators suggested that there was a change in paleolimnological conditions between ~ 1330 cal yrs BP and the present to slightly acidic water chemistry and low electrical conductivity for the B02SR lake. However, for lake 07SR, the alkalinity pattern remained consistent over the past ~ 2500 cal yrs BP.

In the Holocene, stalagmite records from the Pantanal indicated severe reductions in water availability between ~ 3800 and ~ 2100 yrs BP (Bertaux et al., 2002; Novello et al., 2016). Periods with low water availability resulted in subaerial exposure and the development of hiatuses in the strata of the largest floodplain lakes of the Pantanal, as reported for the Gaíva, Mandioré, Cáceres, and Negra lakes between the Middle and Late Holocene (McGlue et al., 2012; Rasbold et al., 2019, 2021). However, most climate proxy records developed from Pantanal floodplain lakes and caves data, suggest increased precipitation over the last millenia (Bertaux et al., 2002; McGlue et al., 2012). Recent studies have indicated that the current salinity of the lower Nhecolândia lakes is not a legacy of past drier climates (Merdy et al., 2022) and that the slope soils act as buffers to store labile species during the dry season, allowing alkalinity to be maintained from a year to the next. However, the alkaline nature of these lakes can quickly disappear after changes in drainage conditions.

Quantified charcoal particles in a floodplain lake on the western edge of the Pantanal, indicated that fires are persistent and recorded with greater intensity and recurrence between the Early and Middle Holocene, which may be related to conditions of lower precipitation and less intense flood pulses compared to the modern conditions (Power et al., 2016). The morphological analysis of the particles indicated that the source vegetation was grasses (elongated geometric shape) and associated with predominantly local burnings in Nhecolândia. Although under climatic conditions of higher humidity, compared to the Early and Middle Holocene, the identification of these charcoal particle depositional peaks indicated episodic droughts in the last millennium that resulted in wildfires.

Thus, the interpretations for cores B02SR and 07SR suggest the formation of an isolated lacustrine environment, between ~ 3080 and ~ 1330 cal yrs BP, under drier conditions than present (Fig. 8). After ~ 1330 cal yrs BP, conditions of water availability increased, and the drainage pattern of B02SR lake underwent changes, resulting in its connection with ephemeral and shallow channels that were activated during floods as distributive channels. Drainage changes provided conditions for B02SR to become a lake with slightly acidic waters and low electrical conductivity, similar to current conditions. For lake 07SR, the drainage pattern was not significantly altered, and the basin remained isolated, which allowed the continuity of the alkaline geochemical pattern from ~ 2500 cal yrs BP to the present (Fig. 2).

Our study provides insights on the paleoecology of a freshwater lake in Nhecolândia, the first record of its kind for the region. Guerreiro et al. (2018) previously reported a chemical transition from freshwater to saline conditions after ~ 1300 cal yrs BP; those authors suggested a climatic control, which was accompanied by nutrient availability and organic matter burial. Results from the present study suggest that saline to freshwater lake transitions also took place over this same period. Additionally, the saline lake in our study maintained its chemistry over the last millennium (Fig. 8). As a consequence, we suggest that the effects of the Late Holocene hydroclimate variability are spatially complex in Nhecolândia, and local geomorphological characteristics of the floodplains, including the distribution of ridges and channels, play an important role in modulating the effects of changing precipitation and evaporation.

Changes in the geochemistry of lakes can have significant implications for carbon source and sink dynamics. Saline and freshwater lakes are responsible for CH_4 gas emissions to the atmosphere (Bergier et al., 2016). However, saline lakes have lower dissolved methane concentrations in their water columns, and their sediment may contain more buried carbon than the freshwater lakes (Bergier et al., 2016). Estimating the regional contribution of greenhouse gas emission and carbon burial in Nhecolândia is a significant challenge due to the wide range of environmental conditions, including high frequency climatic variations, as well as the high salinity and pH levels of surface waters (Bergier et al., 2016; Barbiero et al., 2017). Our sediments cores indicate that the highest rates of organic carbon burial occurred after ~ 1300 cal yrs BP, with similar proportions observed in both saline and freshwater lakes (mean TOC ~ 10–15%). The freshwater lake is colonized by aquatic macrophytes, that contribute considerable biomass to the surface sediment layer (TOC ~ 34%). The sedimentary records of other saline lakes exhibit a similar trend of increasing organic carbon levels over the past millenium (McGlue et al., 2017; Guerreiro et al., 2018). The absence of data from other freshwater lakes limits comparisons of carbon burial in that type. Nonetheless, our study reveals that hydrochemical changes are neither temporally directional nor spatially uniform, which makes estimates of potential changes to greenhouse gas flux difficult to model in this lake district.

Conclusions

In this study, two sediment cores from a freshwater (B02SR) lake and a saline-alkaline (07SR) lake in the lower Nhecolândia region, southern Pantanal (western Brazil), were studied. Our results allowed us to draw the following conclusions:

1) Three sedimentary units were present in the cores. The biological and geochemical indicators suggest the establishment of an alkaline lentic environment in both basins after ~ 3080 cal yrs BP, with the diatom community dominated by *Anomoeoneis* sp. and *Craticula* sp., and high relative K, Mn, Ca, Sr, and Fe in the sediments.
2) The geochemical and biological data from core 07SR indicate chemical stability with consistent alkaline/saline waters; *Nitzschia* sp. and *Craticula* sp. diatom species dominated, and oogonia of *Chara* sp. (Characeae) were routinely encountered in the sediments.
3) A chemical transition from alkaline/saline to freshwater conditions was detected in core B02SR after ~ 1330 cal yrs BP. The shift in the water chemistry was reflected in a change to benthic diatoms *Gomphonema* sp., *Eunotia* sp., *Encyonem*a sp. and *Nitzschia* sp., and the presence of sponge spicules of *Corvoheteromeyenia* spp., *Radiospongilla amazonensis*, *Tubella variabilis* and *Heteromeyenia* sp.
4) This study reveals the complexity of geochemical transitions of Nhecolândia lakes, reveals that they do not uniformly shift towards greater salinity in the last millennium as the hydroclimate of the Pantanal changed. Changes in lake typology is more likely a complex and spatially variable responses to climatic conditions, groundwater levels ,and flow patterns, drainage patterns, soils, and biological metabolism.

Author contributions All authors contributed to the study conception and design. Material preparation, data collection and analysis were performed by GGR, LCRP, PEO, EENA, and DRS. The first draft of the manuscript was written by GGR and all authors commented on previous versions of the manuscript. All authors read and approved the final manuscript.

Funding This work was funded by The São Paulo Research Foundation (FAPESP) (grants 2016/14227–5). G. Rasbold thanks the grants 2020/07726-0 (postdoctoral scholarship).

Data availability The datasets generated during and/or analyzed during the current study are available from the corresponding author on reasonable request.

Declarations

Conflict of interest The authors declare they have no financial interests. The authors declare they have potential conflict of interests.

References

Absy, M., 1975. Polen e esporos do Quaternário de Santos (Brasil). Hoehnea 5: 1–26.

Assine, M., 2003. Sedimentação na Bacia do Pantanal Mato-Grossense, Centro-Oeste do Brasil.

Assine, M. L. & P. C. Soares, 2004. Quaternary of the Pantanal, west-central Brazil. Quaternary International 114(1): 23–34. https://doi.org/10.1016/S1040-6182(03)00039-9.

Barbiero, L., J. P. de Queiroz Neto, G. Ciornei, A. Y. Sakamoto, B. Capellari, E. Fernandes & V. Valles, 2002. Geochemistry of water and ground water in the Nhecolândia, Pantanal of Mato Grosso, Brazil: variability and associated processes. Wetlands 22(3): 528–540. https://doi.org/10.1672/0277-5212(2002)022[0528:GOWAGW]2.0.CO;2.

Barbiero, L., M. Siqueira Neto, R. R. Braz, J. B. D. Carmo, A. T. Rezende Filho, E. Mazzi, F. A. Fernandes, S. R. Damatto & P. B. D. Camargo, 2017. Biogeochemical diversity and hot moments of GHG emissions from shallow alkaline lakes in the Pantanal of Nhecolândia, Brazil. Biogeosciences Discuss 2017: 1–26. https://doi.org/10.5194/bg-2017-108.

Battarbee, R. W., V. J. Jones, R. J. Flower, N. G. Cameron, H. Bennion, L. Carvalho & S. Juggins, 2001. Diatoms. In Smol, J. P., H. J. B. Birks, W. M. Last, R. S. Bradley & K. Alverson (eds) Tracking Environmental Change Using Lake Sediments: Terrestrial, Algal, and Siliceous Indicators. Springer Netherlands, Dordrecht, 155–202. https://doi.org/10.1007/0-306-47668-1_8

Becker, B. F., S. A. F. da Silva-Caminha, R. L. Guerreiro, E. J. de Oliveira, C. D'Apolito & M. L. Assine, 2018. Late Holocene palynology of a saline lake in the Pantanal of Nhecolândia. Brazil. Palynology 42(4): 457–465. https://doi.org/10.1080/01916122.2017.1386843.

Bergier, I., A. Krusche & F. Guérin, 2016. Alkaline Lake Dynamics in the Nhecolândia Landscape. In Bergier, I. & M. L. Assine (eds) Dynamics of the Pantanal Wetland in South America. Springer International Publishing, Cham, 145–161. https://doi.org/10.1007/698_2014_327

Bertaux, J., F. Sondag, R. Santos, F. Soubiès, C. Causse, V. Plagnes, F. Le Cornec & A. Seidel, 2002. Paleoclimatic record of speleothems in a tropical region: study of laminated sequences from a Holocene stalagmite in Central-West Brazil. Quaternary International 89(1): 3–16. https://doi.org/10.1016/S1040-6182(01)00077-5.

Bezerra, M. A., A. A. Mozeto, P. E. Oliveira, C. Volkmer-Ribeiro, V. V. Rodrigues & R. Aravena, 2019. Late Pleistocene/Holocene environmental history of the southern Brazilian Pantanal wetlands. Oecologia Australis 23(04): 712–729.

Blaauw, M. & J. A. Christen, 2011. Flexible paleoclimate age-depth models using an autoregressive gamma process. Bayesian Analysis 6(3):457–474, 18. https://doi.org/10.1214/11-BA618

Bremond, L., A. Alexandre, C. Hély & G. Joel, 2005. A phytolith index as a proxy of tree cover density in tropical areas: Calibration with Leaf Area Index along a forest-savanna transect in southeastern Cameroon. Global and Planetary Change 45: 277–293. https://doi.org/10.1016/j.gloplacha.2004.09.002.

Buso Junior, A. A., L. C. Ruiz Pessenda, P. E. de Oliveira, P. C. Fonseca Giannini, M. C. Lisboa Cohen, C. Volkmer-Ribeiro, S. M. B. de Oliveira, D. De Fátima Rossetti, F. L. Lorente, M. A. Borotti Filho, J. A. Schiavo, J. A. Bendassolli, M. C. França, J. T. Felix Guimarães & G. S. Siqueira, 2013. Late Pleistocene and Holocene Vegetation, Climate Dynamics, and Amazonian Taxa in the Atlantic Forest, Linhares. SE Brazil. Radiocarbon 55(3): 1747–1762. https://doi.org/10.1017/S0033822200048669.

Collinvaux, P., P. Oliveira & J. E. Moreno, 1999. Amazon: Pollen Manual and Atlas: Pollen Manual and Atlas.

Company, M. C., 1975. Munsell soil color charts. Revised edn (Macbeth Division of Kollmorgen, 1994).

Costa, M., K. H. Telmer, T. L. Evans, T. I. R. Almeida & M. T. Diakun, 2015. The lakes of the Pantanal: inventory, distribution, geochemistry, and surrounding landscape. Wetlands Ecology and Management 23(1): 19–39. https://doi.org/10.1007/s11273-014-9401-3.

de Souza Santos, K. R., A. C. R. Rocha & C. L. Sant'Anna, 2012. Diatoms from shallow lakes in the Pantanal of Nhecolândia. Brazilian Wetland. Oecologia Australis 16(4): 756–769.

Faegri, K., P. E. Kaland & K. Krzywinski, 1989. Textbook of pollen analysis. John Wiley & Sons Ltd.

Fornace, K. L., B. S. Whitney, V. Galy, K. A. Hughen & F. E. Mayle, 2016. Late Quaternary environmental change in the interior South American tropics: new insight from leaf wax stable isotopes. Earth and Planetary Science Letters 438: 75–85. https://doi.org/10.1016/j.epsl.2016.01.007.

Fredlund, G. G. & L. T. Tieszen, 1994. Modern Phytolith Assemblages from the North American Great Plains. Journal of Biogeography 21(3): 321–335. https://doi.org/10.2307/2845533.

Furian, S., E. R. C. Martins, T. M. Parizotto, A. T. Rezende-Filho, R. L. Victoria & L. Barbiero, 2013. Chemical diversity and spatial variability in myriad lakes in Nhecolândia in the Pantanal wetlands of Brazil. Limnology and Oceanography 58(6): 2249–2261. https://doi.org/10.4319/lo.2013.58.6.2249.

Furquim, S., Robert Graham, L. Barbiero, Q. Laurent, J. de Neto, Queiroz Neto & P. Vidal-Torrado, 2010. Soil mineral genesis and distribution in a saline lake landscape of the Pantanal Wetland, Brazil. Geoderma (amsterdam) 154: 518–528. https://doi.org/10.1016/j.geoderma.2009.03.014.

Girard, P., I. Fantin-Cruz, S. M. L. de Oliveira & S. K. Hamilton, 2010. Small-scale spatial variation of inundation dynamics in a floodplain of the Pantanal (Brazil). Hydrobiologia 638(1): 223–233. https://doi.org/10.1007/s10750-009-0046-9.

Grimm, E. C., 1987. CONISS: a FORTRAN 77 program for stratigraphically constrained cluster analysis by the method of incremental sum of squares. Computers & Geosciences 13(1): 13–35. https://doi.org/10.1016/0098-3004(87)90022-7.

Guerreiro, R. L., M. M. McGlue, J. R. Stone, I. Bergier, M. Parolin, S. A. F. da Silva Caminha, L. V. Warren & M. L. Assine, 2018. Paleoecology explains Holocene chemical changes in lakes of the Nhecolândia (Pantanal-Brazil). Hydrobiologia 815(1): 1–19. https://doi.org/10.1007/s10750-017-3429-3.

Hammer, O., D. Harper & P. Ryan, 2001. PAST: paleontological Statistics Software Package for Education and Data Analysis. Palaeontologia Electronica 4: 1–9.

Hogg, A. G., T. J. Heaton, Q. Hua, J. G. Palmer, C. S. M. Turney, J. Southon, A. Bayliss, P. G. Blackwell, G. Boswijk, C. Bronk Ramsey, C. Pearson, F. Petchey, P. Reimer, R. Reimer & L. Wacker, 2020. SHCal20 Southern Hemisphere Calibration, 0–55,000 Years cal BP. Radiocarbon 62(4): 759–778. https://doi.org/10.1017/RDC.2020.59.

Hua, Q., J. C. Turnbull, G. M. Santos, A. Z. Rakowski, S. Ancapichún, R. De Pol-Holz, S. Hammer, S. J. Lehman, I. Levin, J. B. Miller, J. G. Palmer & C. S. M. Turney, 2022. Atmospheric radiocarbon for the period 1950–2019. Radiocarbon 64(4): 723–745. https://doi.org/10.1017/RDC.2021.95.

ICPT, I. C. f. P. T., 2019. International Code for Phytolith Nomenclature (ICPN) 2.0. Annals of Botany 124(2):189–199. https://doi.org/10.1093/aob/mcz064

Junk, W. J. & C. N. d. Cunha, 2005. Pantanal: a large South American wetland at a crossroads. Ecological Engineering 24(4):391-401. https://doi.org/10.1016/j.ecoleng.2004.11.012

Keddy, P. A., L. H. Fraser, A. I. Solomeshch, W. J. Junk, D. R. Campbell, M. T. K. Arroyo & C. J. R. Alho, 2009. Wet and Wonderful: the World's Largest Wetlands Are Conservation Priorities. BioScience 59(1): 39–51. https://doi.org/10.1525/bio.2009.59.1.8.

Lacerda Filho, J. V. C. D. B., R.S.; Rodrigues Valente, C.; Cavalcante De Oliveira, C.; Silva, M.G.; Moreton, C.C.; Martins, E.G.; Lopes, R.C.; Muniz Lima, T.; Larizzatti, J.H.; Valente, C.R., 2006. Geologia e recursos minerais do estado de Mato Grosso do Sul: texto explicativo dos mapas geológico e de recursos minerais do estado de Mato Grosso do Sul. Campo Grande: CPRM. Escala 1:1.000.000 Programa Geologia do Brasil - PGB.

Lo, E. L., M. M. McGlue, A. Silva, I. Bergier, K. M. Yeager, H. de Azevedo Macedo, M. Swallom & M. L. Assine, 2019. Fluvio-lacustrine sedimentary processes and landforms on the distal Paraguay fluvial megafan (Brazil). Geomorphology 342: 163–175. https://doi.org/10.1016/j.geomorph.2019.06.001.

Lorente, F. L., L. C. Pessenda, F. Oboh-Ikuenobe, A. A. Buso Jr., M. C. Cohen, K. E. Meyer, P. C. Giannini, P. E. de Oliveira, Rossetti D. de Fátima, M. A. Borotti Filho & M. C. França, 2014. Palynofacies and stable C and N isotopes of Holocene sediments from Lake Macuco (Linhares, Espírito Santo, southeastern Brazil): depositional settings and palaeoenvironmental evolution. Palaeogeography, palaeoclimatology, palaeoecology 415: 69–82. https://doi.org/10.1016/j.palaeo.2013.12.004.

Malone, C. F., K. R. Santos & C. L. Sant'Anna, 2012. Algas E cianobactérias de ambientes extremos do Pantanal BrasileirO. Oecologia Australis 16: 745–755. https://doi.org/10.4257/oeco.2012.1604.02.

McGlue, M. M., R. L. Guerreiro, I. Bergier, A. Silva, F. N. Pupim, V. Oberc & M. L. Assine, 2017. Holocene stratigraphic evolution of saline lakes in Nhecolândia, southern Pantanal wetlands (Brazil). Quaternary Research 88(3): 472–490. https://doi.org/10.1017/qua.2017.57.

McGlue, M. M., A. Silva, M. L. Assine, J. C. Stevaux & F. d. N. Pupim, 2016. Paleolimnology in the Pantanal: Using Lake Sediments to Track Quaternary Environmental Change in the World's Largest Tropical Wetland. In Bergier, I. & M. L. Assine (eds) Dynamics of the Pantanal Wetland in South America. Springer International Publishing, Cham, 51–81. https://doi.org/10.1007/698_2015_350

McGlue, M. M., A. Silva, H. Zani, F. A. Corradini, M. Parolin, E. J. Abel, A. S. Cohen, M. L. Assine, G. S. Ellis & M. A. Trees, 2012. Lacustrine records of Holocene flood pulse dynamics in the Upper Paraguay River watershed (Pantanal wetlands, Brazil). Quaternary Research 78(2): 285–294. https://doi.org/10.1016/j.yqres.2012.05.015.

Merdy, P., M. Gamrani, C. R. Montes, A. T. Rezende Filho, L. Barbiero, D. A. Ishida, A. R. C. Silva, A. J. Melfi & Y. Lucas, 2022. Processes and rates of formation defined by modelling in alkaline to acidic soil systems in Brazilian Pantanal wetland. CATENA 210: 105876. https://doi.org/10.1016/j.catena.2021.105876.

Merino, E. R. & M. L. Assine, 2020. Hidden in plain sight: How finding a lake in the Brazilian Pantanal improves understanding of wetland hydrogeomorphology. Earth Surface Processes and Landforms 45(2): 440–458. https://doi.org/10.1002/esp.4745.

Metcalfe, Sarah E., Bronwen S. Whitney, Katharine A. Fitzpatrick, Francis E. Mayle, Neil J. Loader, F. Alayne Street-Perrott & David G. Mann, 2014. Hydrology and climatology at Laguna La Gaiba, lowland Bolivia: complex responses to climatic forcings over the last 25 000 years. Journal of Quaternary Science 29(3): 289–300. https://doi.org/10.1002/jqs.2702.

Metzeltin, D. & H. Lange-Bertalot, 2007. Tropical diatoms of South America II. Special remarks on biogeographic disjunction. Iconogr Diatomol 18: 1–877.

Meyers, P. A., 1994. Preservation of elemental and isotopic source identification of sedimentary organic matter. Chemical Geology 114(3): 289–302. https://doi.org/10.1016/0009-2541(94)90059-0.

Millspaugh, S. H. & C. Whitlock, 1995. A 750-year fire history based on lake sediment records in central Yellowstone National Park, USA. The Holocene 5(3): 283–292.

Morales, E., C. Wetzel, S. Rivera, M. H. Novais, L. Hoffmann & L. Ector, 2014. *Craticula strelnikoviana* sp. nov. and *Craticula guaykuruorum* sp. nov. (Bacillariophyta) from South American saline lakes. Nova Hedwigia 143: 223–237. https://doi.org/10.1127/1438-9134/2014/010.

Mourão, G., I. Ishii & Z. Campos, 1988. Alguns fatores limnológicos relacionados com a ictiofauna de baías e salinas do Pantanal da Nhecolândia, MS, Brasil. Acta Limnologica Brasiliensia 2: 181–198.

Novello, V. F., F. W. Cruz, M. M. McGlue, C. I. Wong, B. M. Ward, M. Vuille, R. A. Santos, P. Jaqueto, L. C. Pessenda & T. Atorre, 2019. Vegetation and environmental changes in tropical South America from the last glacial to the Holocene documented by multiple cave sediment proxies. Earth and Planetary Science Letters 524: 115717. https://doi.org/10.1016/j.epsl.2019.115717.

Novello, V. F., M. Vuille, F. W. Cruz, N. M. Stríkis, M. S. De Paula, R. L. Edwards, H. Cheng, I. Karmann, P. F. Jaqueto & R. I. Trindade, 2016. Centennial-scale solar forcing of the South American Monsoon System recorded in stalagmites. Scientific Reports 6(1): 1–8. https://doi.org/10.1038/srep24762.

Pessenda, L. C. R., P. E. De Oliveira, M. Mofatto, V. B. de Medeiros, R. J. Francischetti Garcia, R. Aravena, J. A.

Bendassoli, A. Zuniga Leite, A. R. Saad & M. Lincoln Etchebehere, 2009. The evolution of a tropical rainforest/grassland mosaic in southeastern Brazil since 28,000 14C yr BP based on carbon isotopes and pollen records. Quaternary Research 71(3): 437–452. https://doi.org/10.1016/j.yqres.2009.01.008.

Pinheiro, U. & L. Calheira, 2020. Chapter 3 - Phylum Porifera. In Rogers, D. C., C. Damborenea & J. Thorp (eds) Thorp and Covich's Freshwater Invertebrates (Fourth Edition). Academic Press, 79–92. https://doi.org/10.1016/B978-0-12-804225-0.00003-4

Por, F. D., 1995. The Pantanal of Mato Grosso (Brazil): world's largest wetlands, vol 73. Springer Science & Business Media.

Power, M., B. Whitney, F. Mayle, D. Neves, E. de Boer & K. Maclean, 2016. Fire, climate and vegetation linkages in the Bolivian Chiquitano Seasonally Dry Tropical Forest. Philosophical Transactions of The Royal Society B Biological Sciences 371. https://doi.org/10.1098/rstb.2015.0165

Rasbold, G. G., L. Calheira, L. Domingos-Luz, L. C. R. Pessenda, U. Pinheiro & M. M. McGlue, 2023. A morphological guide of neotropical freshwater sponge spicules for paleolimnological studies. Frontiers in Ecology and Evolution 10. https://doi.org/10.3389/fevo.2022.1067432

Rasbold, G. G., M. M. McGlue, J. C. Stevaux, M. Parolin, A. Silva & I. Bergier, 2019. Sponge spicule and phytolith evidence for Late Quaternary environmental changes in the tropical Pantanal wetlands of western Brazil. Palaeogeography, Palaeoclimatology, Palaeoecology 518: 119–133. https://doi.org/10.1016/j.palaeo.2019.01.015.

Rasbold, G. G., M. M. McGlue, J. C. Stevaux, M. Parolin, A. Silva & I. Bergier, 2021. Enhanced middle Holocene organic carbon burial in tropical floodplain lakes of the Pantanal (South America). Journal of Paleolimnology 65(2): 181–199. https://doi.org/10.1007/s10933-020-00159-5.

Rezende-Filho, A., S. Furian, R. Victoria, C. Mascré, V. Valles & L. Barbiero, 2012. Hydrochemical variability at the Upper Paraguay Basin and Pantanal wetland. Hydrology and Earth System Sciences 16: 2723–2737. https://doi.org/10.5194/hess-16-2723-2012.

Roubik, D. & J. E. Moreno, 1991. Pollen and Spores of Barro Colorado Island, vol 47.

Salgado-Labouriau, M. L., 1973. Contribuição à palinologia dos cerrados. Academia Brasileira de Ciências Rio de Janeiro.

Tortato, F. R. & T. J. Izzo, 2017. Advances and barriers to the development of jaguar-tourism in the Brazilian Pantanal. Perspectives in Ecology and Conservation 15(1): 61–63. https://doi.org/10.1016/j.pecon.2017.02.003.

Tremarin, P. I., T. A. V. Ludwig & L. C. Torgan, 2014. Four new Aulacoseira species (Coscinodiscophyceae) from Matogrossense Pantanal Brazil. Diatom Research 29(2): 183–199. https://doi.org/10.1080/0269249X.2014.880072.

Twiss, P., E. Suess & R. Smith, 1969. Morphological Classification of Grass Phytoliths1. Soil Science Society of America Journal - SSSAJ 33. https://doi.org/10.2136/sssaj1969.03615995003300010030x

Wentworth, C. K., 1922. A scale of grade and class terms for clastic sediments. The Journal of Geology 30(5): 377–392.

Whitney, B. S., F. E. Mayle, S. W. Punyasena, K. A. Fitzpatrick, M. J. Burn, R. Guillen, E. Chavez, D. Mann, R. T. Pennington & S. E. Metcalfe, 2011. A 45kyr palaeoclimate record from the lowland interior of tropical South America. Palaeogeography, Palaeoclimatology, Palaeoecology 307(1): 177–192. https://doi.org/10.1016/j.palaeo.2011.05.012.

Zani, H., M. L. Assine & M. M. McGlue, 2012. Remote sensing analysis of depositional landforms in alluvial settings: method development and application to the Taquari megafan, Pantanal (Brazil). Geomorphology 161–162: 82–92. https://doi.org/10.1016/j.geomorph.2012.04.003.